Development/Plasticity/Repair

Asymmetric PI(3,4,5)P_3 and Akt Signaling Mediates Chemotaxis of Axonal Growth Cones

Steven J. Henle,[1] Gordon Wang,[4] Ellen Liang,[2,3] May Wu,[4] Mu-ming Poo,[4] and John R. Henley[1,2,3]

[1]Mayo Graduate School, College of Medicine, and Departments of [2]Neurologic Surgery and [3]Physiology and Biomedical Engineering, Mayo Clinic, Rochester, Minnesota 55905, and [4]Division of Neurobiology, Department of Molecular and Cell Biology, Helen Wills Neuroscience Institute, University of California, Berkeley, California 94720

The action of many extracellular guidance cues on axon pathfinding requires Ca^{2+} influx at the growth cone (Hong et al., 2000; Nishiyama et al., 2003; Henley and Poo, 2004), but how activation of guidance cue receptors leads to opening of plasmalemmal ion channels remains largely unknown. Analogous to the chemotaxis of amoeboid cells (Parent et al., 1998; Servant et al., 2000), we found that a gradient of chemoattractant triggered rapid asymmetric PI(3,4,5)P_3 accumulation at the growth cone's leading edge, as detected by the translocation of a GFP-tagged binding domain of Akt in *Xenopus laevis* spinal neurons. Growth cone chemoattraction required PI(3,4,5)P_3 production and Akt activation, and genetic perturbation of polarized Akt activity disrupted axon pathfinding *in vitro* and *in vivo*. Furthermore, patch-clamp recording from growth cones revealed that exogenous PI(3,4,5)P_3 rapidly activated TRP (transient receptor potential) channels, and asymmetrically applied PI(3,4,5)P_3 was sufficient to induce chemoattractive growth cone turning in a manner that required downstream Ca^{2+} signaling. Thus, asymmetric PI(3,4,5)P_3 elevation and Akt activation are early events in growth cone chemotaxis that link receptor activation to TRP channel opening and Ca^{2+} signaling. Altogether, our findings reveal that PI(3,4,5)P_3 elevation polarizes to the growth cone's leading edge and can serve as an early regulator during chemotactic guidance.

Introduction

Soon after discovering the axonal growth cone, Ramón y Cajal suggested that factors secreted from target cells may attract developing axons in a manner similar to cell chemotaxis (Ramón y Cajal, 1972). Many secreted axon guidance factors and their cognate receptors have since been identified (Tessier-Lavigne and Goodman, 1996), but key elements of the transduction mechanisms underlying growth cone chemotaxis remain outstanding. Several guidance cues induce Ca^{2+} signals in the growth cone, and asymmetric Ca^{2+} elevation elicits growth cone turning (Zheng, 2000; Henley and Poo, 2004; Henley et al., 2004). In particular, both growth cone attractive turning and Ca^{2+} influx induced by brain-derived neurotrophic factor (BDNF) and netrin-1 require activation of TRP channels (Li et al., 2005; Wang and Poo, 2005). The activation of TRP channels can be regulated by many mechanisms, including membrane insertion (Bezzerides et al., 2004), channel phosphorylation (Ramsey et al., 2006), phosphoinositides (Kwon et al., 2007), and proline isomerization (Shim et al., 2009). However, the signaling intermediates linking guidance receptor activation and TRP channel opening at the growth cone surface has remained unknown.

The phosphoinositides are important signaling lipids. Phosphoinositide 3-kinase (PI3K) phosphorylates PI(4,5)P_2 to cause a dynamic increase in the relatively lower level of PI(3,4,5)P_3 in the inner leaflet of the plasmalemmal bilayer (Di Paolo and De Camilli, 2006). Elevated PI(3,4,5)P_3 elicits the recruitment and activation of a number of effector proteins, including the downstream kinase Akt. Polarized elevation of PI(3,4,5)P_3 mediates the detection of chemoattractant gradients during chemotaxis of *Dictyostelium* and neutrophils (Parent et al., 1998; Servant et al., 2000; Wang et al., 2002). Intriguingly, perturbing PI3K function disrupts axon guidance (Ming et al., 1999; Chang et al., 2006; Wolf et al., 2008; Akiyama and Kamiguchi, 2010). However, the spatiotemporal profile of PI(3,4,5)P_3 elevation in the growth cone, the role of downstream effectors like Akt, and the link between PI(3,4,5)P_3 and Ca^{2+} signaling during chemotactic growth cone guidance has remained completely unknown.

Here we report for the first time that polarized PI(3,4,5)P_3 elevation and Akt signaling mediate growth cone detection of chemoattractive guidance cues. In cultures of *Xenopus* spinal neurons, chemoattractive turning of growth cones induced by netrin-1 and BDNF required Akt activity, and a gradient of BDNF rapidly triggered the accumulation of PI(3,4,5)P_3 at the growth cone's leading edge, as revealed by the translocation of a GFP-

Received Jan. 13, 2011; revised March 8, 2011; accepted March 17, 2011.

Author contributions: S.J.H., G.W., M.-m.P., and J.R.H. designed research; S.J.H., G.W., E.L., M.W., and J.R.H. performed research; S.J.H., G.W., E.L., M.W., and J.R.H. analyzed data; S.J.H., G.W., M.-m.P., and J.R.H. wrote the paper.

This work was supported by a John M. Nasseff, Sr., career development award from the Mayo Clinic (J.R.H.), the National Institutes of Health (NIH) (J.R.H.; M.-m.P.), and a Robert D. and Patricia E. Kern Predoctoral Fellowship award (S.J.H.). We thank S. Wong (University of California, Berkeley) for discussions, T. Balla (NIH) for the gift of the PH_{Akt}-GFP construct, S. Ekker (Mayo Clinic) for the DsRed RNA expression vector, T. Gomez (University of Wisconsin, Madison) and G. Sieck (Mayo Clinic) for assistance with *in vivo* imaging, M. Tessier-Lavigne (Genentech) for providing netrin-1, and A. Windebank (Mayo Clinic) for sharing laboratory space.

The authors declare no competing financial interests.

Correspondence should be addressed to John R. Henley, Department of Neurologic Surgery, Mayo Clinic, 200 First Street SW, Rochester, MN 55905. E-mail: henley.john@mayo.edu.

G. Wang's present address: Department of Molecular and Cell Physiology, Stanford University, Stanford, CA 94305.

E. Liang's present address: University of Minnesota Medical School, Minneapolis, MN 55455.

DOI:10.1523/JNEUROSCI.0216-11.2011

 0270-6474/11/317016-12$15.00/0

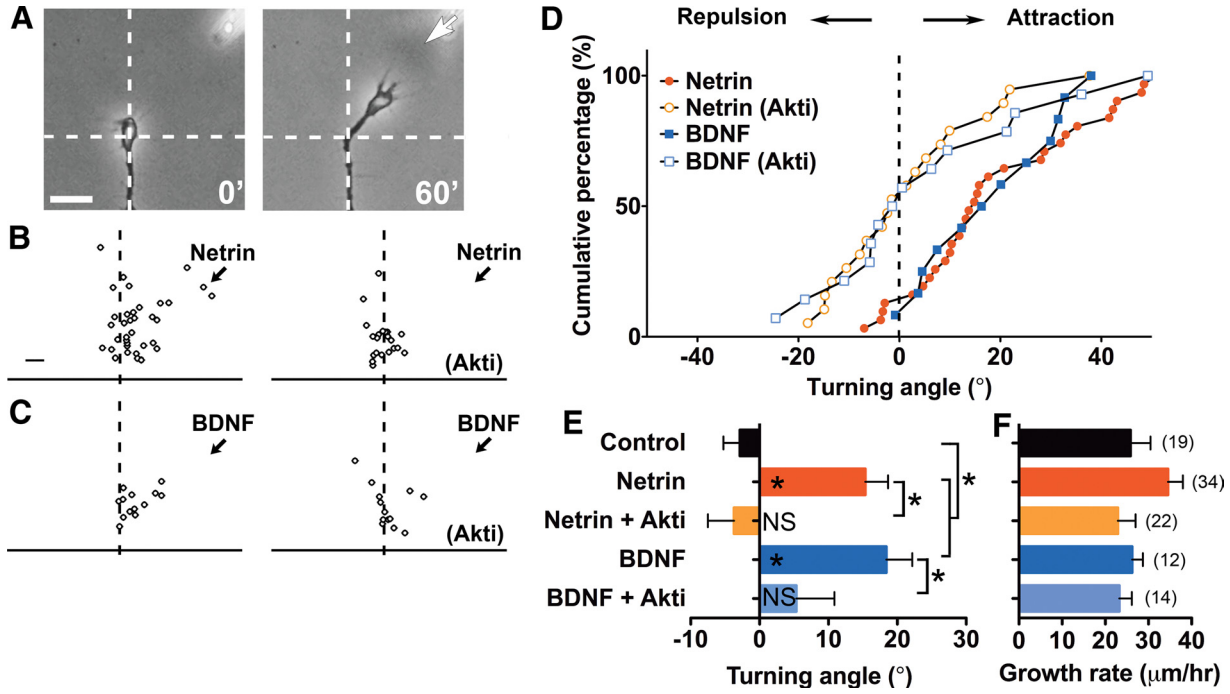

Figure 1. Essential role of $PI(3,4,5)P_3$ and Akt during axonal growth cone chemoattraction. ***A***, Example images of a *Xenopus* spinal neuron growth cone at the onset (left) and end (right) of a 1 h exposure to a gradient of netrin-1, which was applied from a micropipette positioned at 45° from the initial direction of growth (5 μg/ml in the pipette; see Materials and Methods). The arrow indicates the direction of the gradient. Scale bar, 20 μm. ***B***, ***C***, Summary plot shows the final position of the growth cone relative to the starting position (origin) for all experiments after 1 h treatment with a gradient of netrin-1 (***B***) or BDNF (***C***, 50 μg/ml in the pipette) in the absence or presence of Akti (5 μM). Scale bar, 10 μm. ***D***, The distribution of turning angles for each set of data shown in ***B*** and ***C***. For each experimental condition, the angular position of the growth cone at the end of a 1 h exposure to a gradient of netrin-1 or BDNF is shown in the cumulative distribution plot. The data points depict the percentage of growth cones with a turning angle less than or equal to a given angular value. ***E***, ***F***, Mean turning angles (***E***) and growth rates (***F***) from all experiments showing the effects of Akti (5 μM) on growth cone turning induced by a gradient of a control solution, netrin-1, or BDNF. Data are the mean ± SEM (n = number in the parentheses). *$p < 0.02$, Mann–Whitney U test.

tagged $PI(3,4,5)P_3$-binding domain of Akt (PH_{Akt}-GFP). A gradient of exogenous $PI(3,4,5)P_3$ was also sufficient to induce attractive growth cone turning. Uniform elevation of Akt activity in the nervous system of *Xenopus* embryos disrupted axon pathfinding *in vivo*. Growth cone guidance by $PI(3,4,5)P_3$ required both TRP channel function and downstream Ca^{2+} signaling. Furthermore, patch-clamp analysis revealed that $PI(3,4,5)P_3$ and Akt positively regulate TRP channel-dependent Ca^{2+} influx at the growth cone. Together, these findings reveal the essential role of asymmetric $PI(3,4,5)P_3$ elevation and Akt activation in the transduction mechanism linking guidance receptors to cytoplasmic Ca^{2+} signaling during growth cone chemotaxis.

Materials and Methods

Primary cell culture of Xenopus *spinal neurons.* We maintained wild-type *Xenopus laevis* (Nasco and Xenopus One) in approved animal facilities (UC Berkeley and Mayo Clinic) according to institutional guidelines. *In vitro* fertilization and dissociated cell culture from stage 22 embryos of either sex were described previously (Zheng et al., 1994; Henley et al., 2004). We plated cells onto coverglass 14 h before experimentation. Reagents were from Sigma unless indicated otherwise.

Quantitative assay of growth cone turning. Calibrated micropipettes produced microscopic gradients resulting in a 1000-fold concentration decrease at the growth cone compared to the solution in the pipette, as described previously (Zheng et al., 1994). The micropipettes contained netrin-1 (5 μg/ml; M. Tessier-Lavigne, Genentech, South San Francisco, CA), BDNF (50 μg/ml; Peprotech), synthetic $PI(3,4,5)P_3$ with neomycin carrier (400 and 266 μM, respectively; Echelon), or ionomycin (1 μM; Calbiochem). Pharmacological agents were applied as stated in the figure legends for 15 min before the start of the assay at the following concentrations: 3.33 μM LY294002, 5 μM Akti, or 1 μM BAPTA-AM. We monitored neurite growth for 15 min to determine the initial direction of extension, and the micropipette was positioned at a 45° angle relative to this initial direction of extension. After 1 h, we measured the change in direction of extension relative to the initial trajectory.

Quantitative immunofluorescence analyses of Akt function. Spinal neuron cultures were first fixed in PBS with 4% formaldehyde, permeabilized with 0.1% Triton X-100, and blocked with 5% goat serum. Cultures were then stained with primary antibodies against phospho-Akt (16.7 μg/ml, Rockland, 600-401-268), phospho-Akt substrate (10 μg/ml, Cell Signaling Technology, 9611), and/or HA (10 μg/ml, Cell Signaling Technology, 2367) and the appropriate Alexa dye-labeled secondary antibodies (4 μg/ml, Invitrogen). Last, we stained for total protein using 5-(4,6-dichlorotriazinyl)aminofluorescein (20 μM, DTAF, Invitrogen). We obtained images using a Zeiss 5-LIVE with 100× 1.4 NA objective. ImageJ (NIH) software was used to determine the mean thresholded fluorescence intensity within a region of interest containing the growth cone. CA-Akt expression was determined based on HA fluorescence. Values for phosphorylated Akt (pAkt) and Akt substrate phosphorylation site (pSub) were normalized to DTAF values in the same region of interest to control for fluctuations in protein levels in the growth cone. All values were normalized to the appropriate control condition.

Embryo injections and live-cell imaging. We injected embryos at the two- to four-cell stage with ~10 nl of DNA encoding the $PI(3,4,5)P_3$ biosensor PH_{Akt}-GFP (200 ng/ml; T. Balla, National Institutes of Health, Bethesda, MD). Some embryos were coinjected with rhodamine-dextran (250 μM; Invitrogen) as a general cytoplasmic tracer. Embryos with PH_{Akt}-GFP-expressing spinal cords were selected for culture at stage 22. We plated neurons on coverglass bottom dishes for confocal imaging (Zeiss 5-LIVE and Leica TCS SP) and collected images at 20 s intervals throughout the experiment, starting 2 min before treatment with BDNF, exogenous $PI(3,4,5)P_3$, or control solutions as indicated in the figure legends. Overexpression of PH_{Akt}-GFP can act as a dominant-negative inhibitor of Akt function, which precludes its utility for functional assays (Akiyama and Kamiguchi, 2010). We chose growth cones with low PH_{Akt}-GFP expression that had maintained filopodial activity for the imaging experiments. Gradient applications were from a micropipette

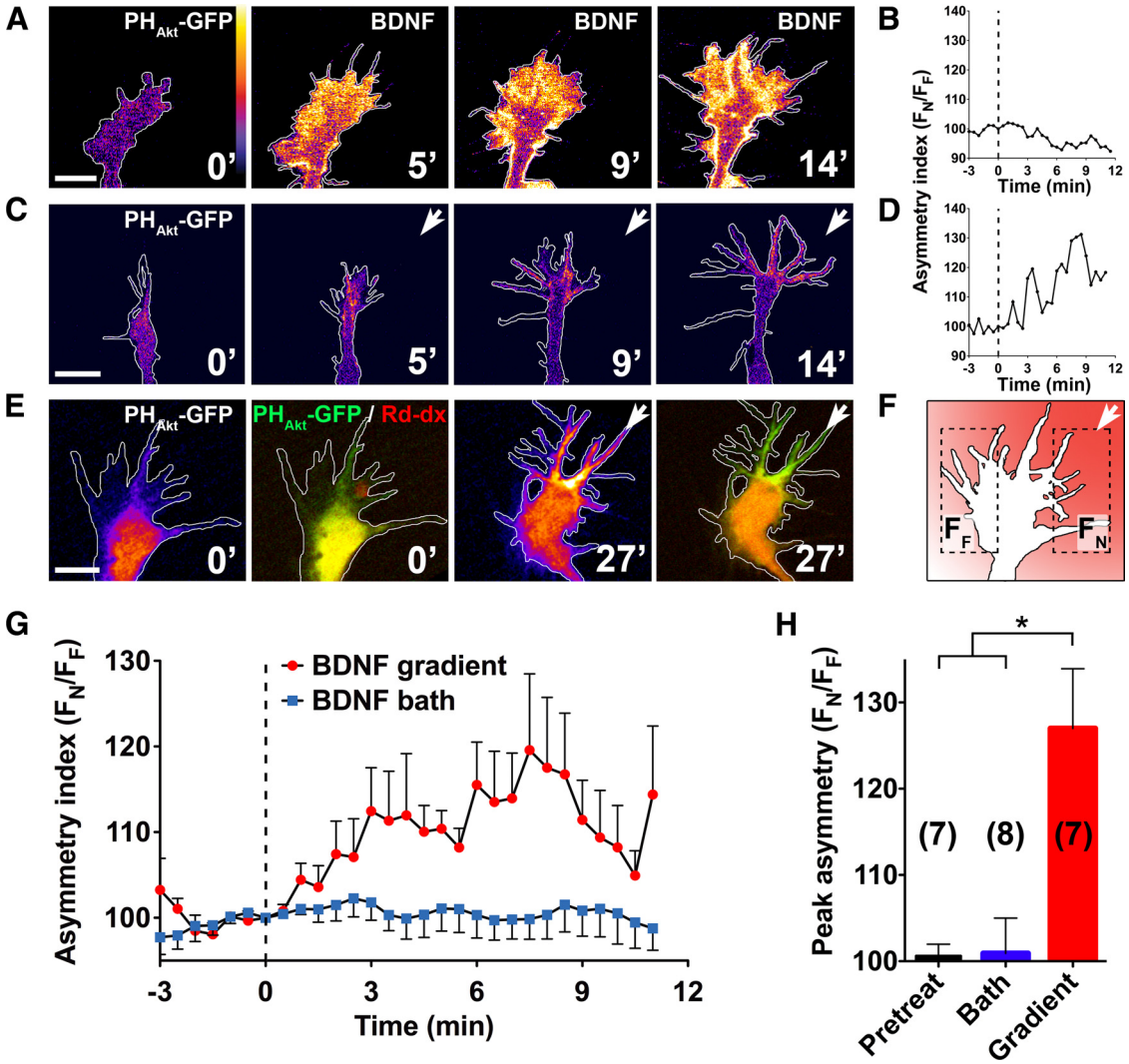

Figure 2. Chemoattractant-induced $PI(3,4,5)P_3$ signals in the growth cone. ***A–E***, BDNF-induced changes in $PI(3,4,5)P_3$ localization in response to uniform (***A***, ***B***) or gradient (***C–E***) application of BDNF. ***A***, ***C***, ***E***, Time-lapse confocal images of growth cones expressing PH_{Akt}-GFP before and after uniform BDNF application (***A***, 50 ng/ml) or application of a gradient of BDNF (***C***, ***E***, 50 ng/ml at the growth cone). Arrows mark the direction of the gradient, and time (in minutes) is indicated in each frame. Pseudocolor scale indicates GFP fluorescence level with black and white representing lowest and highest intensities, respectively. ***E***, Pseudocolor images represent the PH_{Akt}-GFP signal before (0′) and after (27′) gradient application of BDNF. Corresponding double-labeled images show both the PH_{Akt}-GFP (green) and cytoplasmic marker rhodamine-dextran (red; Rd-dx). Scale bar, 10 μm. ***B***, Quantitative measurements of fluorescence asymmetry comparing $PI(3,4,5)P_3$ signals on opposite sides of the growth cone in ***A***, which was treated with uniform application of BDNF. Note that although intensity levels increase after treatment, BDNF application has no effect on the left–right polarity of $PI(3,4,5)P_3$ signals. ***D***, Fluorescence asymmetry measurements of the growth cone in ***C***, which was exposed to a gradient of BDNF. Note that the asymmetric $PI(3,4,5)P_3$ localization fluctuates but peaks at 8–9 min in this example. ***F***, Schematic demonstrating how quantitative fluorescence asymmetry measurements were made by comparing fluorescence intensity on the near (F_N) and far (F_F) sides of the growth cone relative to the gradient source. ***G***, Summary of all growth cones measured as in ***B***, ***D***, and ***F***. Images were collected every 20 s for each growth cone treated with either a BDNF gradient (red) or a uniform application of BDNF (50 ng/ml; blue) starting at time 0. Data are the mean ± SEM ($n = 7$ for pretreatment and gradient application and 8 for bath application). $p < 0.0001$, repeated-measures two-way ANOVA. ***H***, The mean peak asymmetry (F_N/F_F) of all growth cones before gradient treatment (pretreat) and during uniform (bath) and gradient (gradient) application of BDNF shown in ***G***. Data are the mean ± SEM (n = number in the parentheses). *$p < 0.01$, two-tailed Student's t test. See also Movies 1 and 2.

positioned at a 45° angle relative to the long axis of the growth cone to recapitulate the conditions used for the quantitative assays of growth cone turning. For image analysis (ImageJ, NIH), we thresholded the gray level above background levels and measured the mean fluorescence intensity for pixels in regions of interest containing the third of the growth cone nearest (F_N) and farthest (F_F) from the pipette, respectively (Henley et al., 2004). We then calculated the asymmetry index ($F_N/F_F \times 100$) for each time point for every growth cone.

Assays of axon guidance in vivo. Messenger RNA was transcribed *in vitro* (mMessage machine, Ambion) from linearized plasmid pSP64 DNA (16244; Addgene) encoding the HA-CA-Akt sequence (Zhou et al., 2000) and pT3TS plasmid DNA encoding DsRed (S. Ekker, Mayo Clinic, Rochester, MN). A single cell of four- to eight-cell stage embryos was injected with ~10 nl mRNA encoding either HA-CA-Akt (1.5 μg/ml) or DsRed (1.5 μg/ml) so that expression was limited to one side of the dorsal spinal cord. Spinal cords were prepared for imaging as previously described (Moon and Gomez, 2005). Stage 27 embryos were fixed overnight in a PBS solution containing 4% formaldehyde and 4% sucrose. After dissection, the spinal cords were permeabilized and washed before incubating overnight with primary antibodies against neurofilament-associated antigen (1:25; 3A10, Iowa Hybridoma Database) and anti-HA (4 μg/ml; ab9110, Abcam). Secondary antibodies (8 μg/ml; Alexa 488 and 594, Invitrogen) were applied for 2 h. Spinal cords were pinned and imaged with a Bio-Rad confocal microscope using a 20× NA 0.5 water-immersion objective. Antibody 3A10 labels commissural axons that originate in both sides of the spinal cord and then cross the midline to the contralateral side. Therefore, 3A10-immunopositive axons that were double labeled with anti-HA or DsRed, respectively, were selected for analysis since these axons originated from one side only (the injected side) and crossed the midline in the same direction. Images were ana-

lyzed using ImageJ software (NIH). The approach angle and crossing angle were measured as the angle an axon deviated from a line perpendicular to the midline in a 30 μm region approaching the midline, or a 60 μm region centered on the midline, respectively. For these measurements, a line perpendicular to the midline was set as 0°, and axons that had turned anteriorly were defined as positive, whereas those that had turned posteriorly were defined as negative. For Figure 4*D*, the mean absolute value of the approach angles is shown to demonstrate the change in deviation from perpendicular.

Electrophysiology. Whole-cell recordings using amphotericin B perforation were made on the growth cone of *Xenopus* spinal neurons, using a patch-clamp amplifier (Axopatch 200B, Molecular Devices). Recording pipettes had resistances of 5–8 MΩ and were filled with an internal solution consisting of (in mM) 125 K^+ gluconate, 20 KCl, 10 HEPES, 0.2 EGTA, 1 $MgCl_2$, and 1 NaCl, adjusted to pH 7.4 with KOH and an osmolarity of 290–296 mOsm. We added amphotericin B (200 μg/ml) to the internal solution immediately before recording. The bathing solution contained the following (in mM): 140 NaCl, 35 TEA-Cl, 1 $CaCl_2$, 10 HEPES. In experiments that determined the *I*/*V* relationship, we isolated the putative TRP current with a modified internal solution. The modified internal solution replaced K^+ gluconate and KCl with CsCl, and the following blockers of voltage-dependent Na^+ and Ca^{2+} (VDCC) channels were added in the bath: TTX (1 μM; Na^+ channel), calcicludine (200 nM; L-, N-, P-type VDCC; Calbiochem) (Schweitz et al., 1994), Ni^{2+} (50 μM; T-type VDCC), mibefradil (5 μM; T-type VDCC), and pimozide (70 μM; T-type VDCC). For measurement of *I*/*V* characteristics, step depolarizations (10 mV, 100 ms) from a holding membrane potential of −60 to +90 mV or a 100 ms voltage ramp from −60 to +40 mV were generated using P-Clamp 8.0 (Molecular Devices). Data were collected at 10 kHz and filtered at 2 kHz. A second micropipette was used for focal application of netrin-1 or synthetic $PI(3,4,5)P_3$ mixed with the neomycin sulfate carrier solution (resulting in concentration of 5 ng/ml and 400 nM at the growth cone, respectively).

Morpholino knockdown. A morpholino oligonucleotide designed to target a 25 nt sequence in the 5′UTR of the reported gene sequences of *Xenopus* TRP-1 (Bobanovic et al., 1999; Brereton et al., 2000) (5′-CTCTGATAAAGAGCAGCCATGATGA) and a control morpholino oligonucleotide based on this sequence with 5 randomized (misprimed) nucleotides (5′-CTgTcATAAAGAcCAGgCATcATGA) or standard control morpholino (Ctrl MO) (5′-CCTCTTACCTCAGTTACAATTTATA) were from Genetools. These morpholino oligonucleotides were conjugated to lissamine for verification using fluorescence microscopy. The neurons were loaded with these morpholino oligonucleotides by early embryo injection following the method previously described (Wang and Poo, 2005).

Statistical analysis. Data were analyzed with GraphPad Prism software (v5). The figure legends state the statistical tests used. Statistical comparisons involving turning assay experiments and *in vivo* turning measurements used the Mann–Whitney *U* test due to the nonparametric distribution of the data. For all other data with a normal distribution, statistical comparisons used the two-tailed Student's *t* test (see Figs. 2*C*, 6) and repeated-measures two-way ANOVA (see Fig. 2*B*).

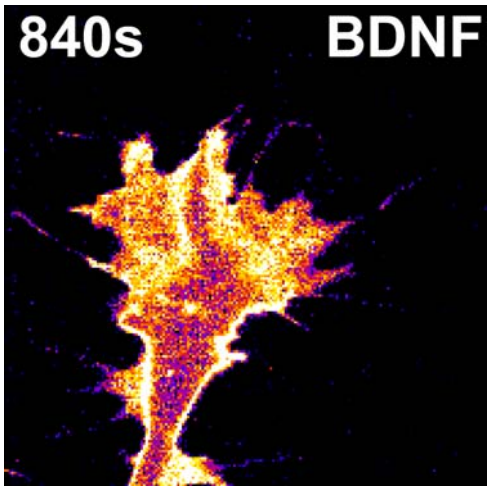

Movie 1. Time-lapse confocal images of a *Xenopus* spinal neuron growth cone expressing PH_{akt}-GFP (pseudocolor). Uniform application of BDNF begins at time = 0 s and induces rapid translocation of the PH_{akt}-GFP biosensor to the growth cone plasmalemma. Note that the signal distribution fluctuates but does not persist in any direction. Selected images from this movie are shown in Figure 2*A*.

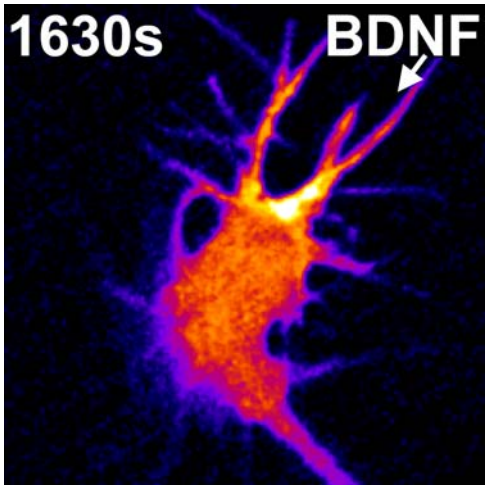

Movie 2. Time-lapse confocal images of a *Xenopus* spinal neuron growth cone expressing PH_{akt}-GFP (pseudocolor). An example movie of a growth cone treated with a BDNF gradient (arrow). In this example, the growth was imaged for a longer time period (in seconds) during gradient application and has initiated a turn toward the BDNF source. Note that the asymmetric PH_{akt}-GFP translocation persists past 25 min after starting the BDNF gradient. Selected images from this movie are shown in Figure 2*E*.

Results

Requirement of $PI(3,4,5)P_3$ and Akt signaling during growth cone chemoattraction

We examined the role of $PI(3,4,5)P_3$ and Akt signaling in growth cone chemoattraction induced by extracellular guidance cues, using cultured *Xenopus* spinal neurons and a quantitative assay of growth cone turning and extension (Zheng et al., 1994). Consistent with previous findings (Song et al., 1997; Ming et al., 1999), pulsatile ejection of netrin-1 or BDNF from a calibrated micropipette produced a microscopic gradient of these factors that led to significant growth cone chemoattraction compared to a control solution (Fig. 1*A–E*). Uniform bath application of a cell permeant inhibitor of Akt (Akt inhibitor 3, abbreviated "Akti"; 5 μM) (Kozikowski et al., 2003) abolished growth cone chemoattraction induced by BDNF and netrin-1 (Fig. 1*B–E*). The rate of axon extension was unaffected by the Akt inhibitor at the concentration used for turning assays (Fig. 1*F*), but higher doses of Akti slowed outgrowth (data not shown). These results indicate that growth cone chemoattraction induced by these guidance factors requires $PI(3,4,5)P_3$ production and Akt activation.

Polarization of $PI(3,4,5)P_3$ during growth cone chemoattraction

To determine the spatiotemporal pattern of $PI(3,4,5)P_3$ signals during growth cone chemoattraction, we expressed a biosensor fusion protein comprising the $PI(3,4,5)P_3$ binding PH-domain of Akt fused to GFP (Várnai and Balla, 1998) in developing *Xenopus* embryos (Fig. 2). Confocal imaging of cultured myocytes revealed that the expressed fusion protein exhibited a diffuse cytoplasmic distribution that translocated to the plasmalemma in response to the elevated

$PI(3,4,5)P_3$ in the membrane induced by insulin (Toker and Cantley, 1997; Servant et al., 2000; Wang et al., 2002) (data not shown). We used this approach to monitor $PI(3,4,5)P_3$ in spinal neuron growth cones. Uniform bath application of BDNF triggered translocation of the diffuse cytoplasmic PH_{Akt}-GFP to the plasmalemma within minutes, indicating accumulation of plasmalemmal $PI(3,4,5)P_3$. The PH_{Akt}-GFP translocation showed a global plasmalemmal distribution with stochastic fluctuations (Fig. 2*A*, Movie 1). When a microscopic gradient of BDNF was applied to individual growth cones, the cytoplasmic PH_{Akt}-GFP appeared to translocate to the surface membrane in a polarized manner: the PH_{Akt}-GFP translocation fluctuated but in general showed a preferential elevation on the side nearer the source of the BDNF gradient (Fig. 2*C*,*E*, Movie 2). Growth cones expressing PH_{Akt}-GFP and double labeled with the fluorescent cytoplasmic tracer rhodamine-dextran (Rd-dx) confirmed that the PH_{Akt}-GFP signal became less cytoplasmic and more enriched in the plasmalemma during the BDNF gradient (Fig. 2*E*). Imaging for a longer time period revealed that the preferential elevation on the side nearer to the gradient source persisted for >25 min (Fig. 2*E*).

To analyze the distribution of the PH_{Akt}-GFP biosensor across the growth cone, we made quantitative ratiometric measurements and compared the mean fluorescence intensity at the near (F_N; closer to the source of BDNF) versus the far (F_F) side of the growth cone (Fig. 2*F*, see Materials and Methods). Analysis of an example growth cone during uniform BDNF application showed a relatively even distribution of the PH_{Akt}-GFP biosensor on both sides of the growth cone (Fig. 2*B*). In contrast, a growth cone treated with a BDNF gradient had a higher elevation of PH_{Akt}-GFP on the side of the growth cone nearer the gradient source (Fig. 2*D*). Similar analysis of all growth cones treated with uniform or gradient application of BDNF confirmed a significant difference in the asymmetry of the PH_{Akt}-GFP signal between the treatment conditions (Fig. 2*G*) (repeated-measures two-way ANOVA). Measurements of peak asymmetry (F_N:F_F, see Materials and Methods) for each growth cone demonstrated a significant difference in the spatial distribution of $PI(3,4,5)P_3$ signals induced by a gradient of BDNF (127.0 ± 6.9% SEM) compared to a uniform concentration of BDNF (100.9 ± 4.1% SEM) or before gradient application (100.6 ± 1.4 SEM; $p < 0.01$, Student's *t* test) (Fig. 2*H*). Thus, analogous to chemotaxis of amoeboid cells, $PI(3,4,5)P_3$ accumulation in the growth cone plasmalemma is polarized toward the source of chemoattractant gradient.

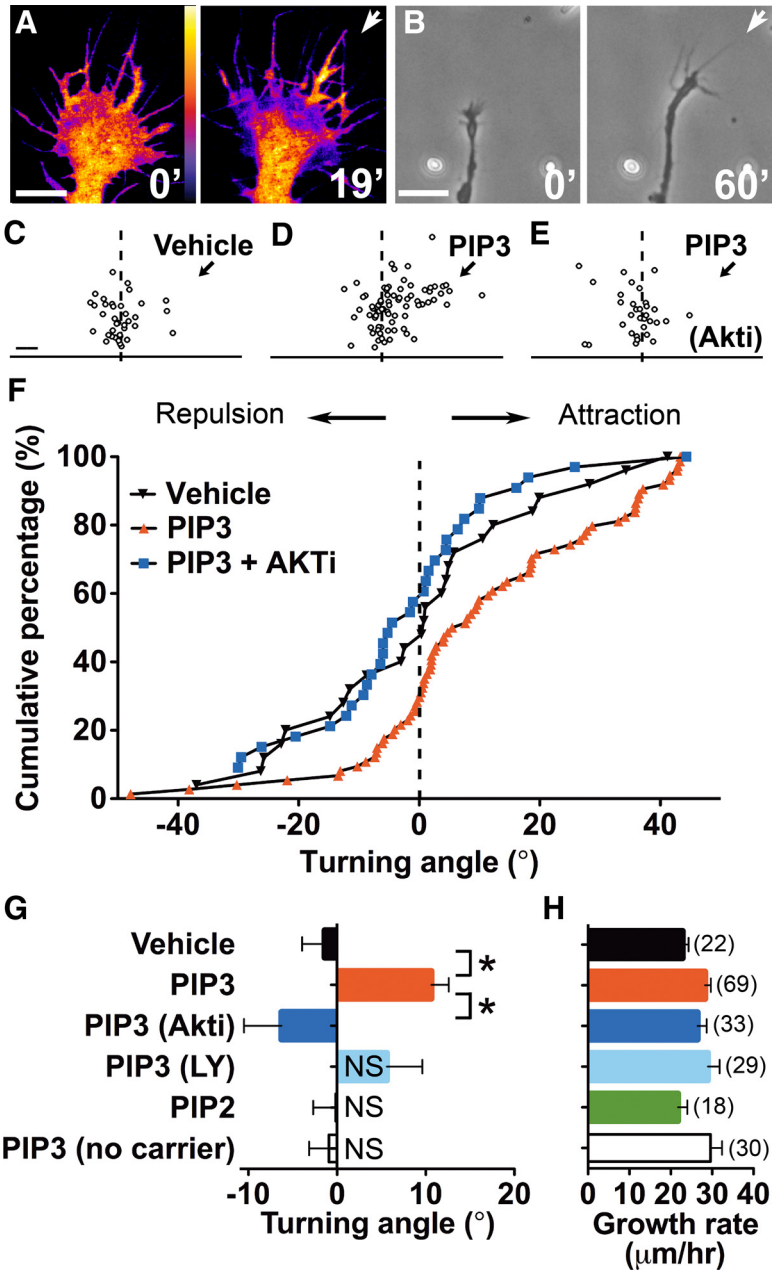

Figure 3. Growth cone chemoattractive turning induced by a gradient of $PI(3,4,5)P_3$. ***A***, Confocal images show asymmetric translocation of PH_{Akt}-GFP from the cytoplasm to the growth cone plasmalemma during application of a gradient of $PI(3,4,5)P_3$ in a carrier solution from a micropipette (400 μM $PI(3,4,5)P_3$ in the pipette). Values indicate the time (in minutes) after the onset of application. Pseudocolor scale indicates GFP fluorescence level: white is higher and black is lower. Scale bar, 10 μm. ***B***, Representative images of a growth cone before (left) and after (right) a 1 h exposure to a gradient of exogenous $PI(3,4,5)P_3$ from a micropipette (arrow). Scale bar, 40 μm. ***C–E***, Summary plots indicate the final position of the growth cone relative to the starting position (origin) for all experiments after 1 h treatment with either a gradient of carrier solution alone (***C***, 266 μM neomycin sulfate), a gradient of carrier solution with exogenous $PI(3,4,5)P_3$ [***D***, 400 μM $PI(3,4,5)P_3$], or a gradient of carrier solution with exogenous $PI(3,4,5)P_3$ during treatment with Akti (5 μM) (***E***). The arrow marks the position of the pipette. Scale bar, 20 μm. ***F***, Cumulative distribution of growth cone turning angles plotted for each set of data in ***C–E***. ***G***, ***H***, Mean turning angles (***G***) and growth rates (***H***) from all experiments showing the effects of the PI3K inhibitor LY294002 (LY; 3.33 μM) and Akti, on growth cone turning induced by a gradient of exogenous $PI(3,4,5)P_3$. Also shown are the effects of no carrier with the $PI(3,4,5)P_3$ (400 μM) gradient and a gradient of exogenous $PI(4,5)P_2$ (400 μM) plus carrier (266 μM neomycin sulfate) on growth cone turning. Data are the mean ± SEM (*n* = number in the parentheses). *$p < 0.02$; NS, not significant compared to vehicle control, Mann–Whitney *U* test.

Growth cone steering by exogenous $PI(3,4,5)P_3$

Is asymmetric accumulation of $PI(3,4,5)P_3$ alone sufficient to induce growth cone turning? We addressed this question directly by applying a microscopic gradient of exogenous $PI(3,4,5)P_3$ in a solution containing a carrier molecule that enables its incorporation into the

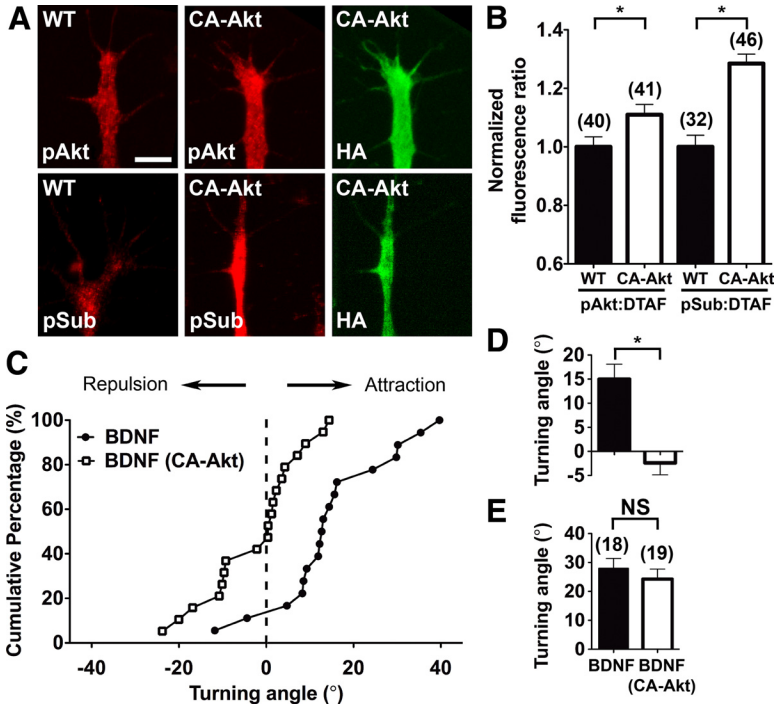

Figure 4. Dysregulation of Akt signaling leads to loss of attraction to BDNF. ***A***, Immunofluorescence images of *Xenopus* growth cones immunostained for pAkt (top, red), pSub, (bottom, red), or anti-HA to detect CA-Akt expression (HA, right, green). Scale bar, 20 μm. ***B***, Average fluorescence ratio of pAkt or pSub to the total protein stain DTAF. *$p < 0.05$, two-tailed Student's *t* test. ***C***, Cumulative distribution of growth cone turning angles in response to a gradient of BDNF with or without CA-Akt expression. ***D***, ***E***, Mean turning angles (***D***) and growth rates (***E***) from all experiments shown in ***C***. Data are the mean ± SEM (n = number in the parentheses). *$p < 0.05$; NS, not significant, Mann–Whitney *U* test.

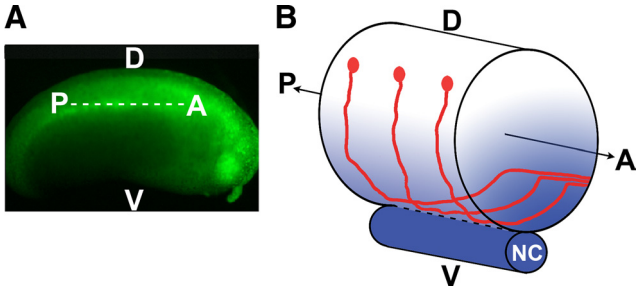

Figure 5. Axon guidance at the midline *in vivo*. ***A***, A stage 22 *Xenopus* embryo expressing GFP in the spinal cord. A, Anterior; P, posterior; D, dorsal; V, ventral. ***B***, A schematic diagram of a *Xenopus* spinal cord and notochord (NC). Commissural interneurons (red) with cell bodies located in the dorsal spinal cord project axons ventrally, which cross the midline and turn rostrally.

inner leaflet of the plasmalemma (see Materials and Methods) (Ozaki et al., 2000; Wang et al., 2002). When a gradient of exogenous $PI(3,4,5)P_3$ together with the carrier was applied to a growth cone expressing the $PI(3,4,5)P_3$ biosensor PH_{Akt}-GFP, we observed a marked asymmetric translocation of PH_{Akt}-GFP to the plasmalemma (Fig. 3*A*). This indicates that the exogenous $PI(3,4,5)P_3$ is able to incorporate into the cytoplasmic side of the growth cone plasmalemma. Similar application of a solution containing the carrier alone caused no detectable PH_{Akt}-GFP translocation (data not shown). Remarkably, application of the exogenous $PI(3,4,5)P_3$ gradient triggered significant growth cone attraction, whereas a gradient of the carrier alone had no effect (Fig. 3*B–D,F,G*). A gradient of exogenous $PI(3,4,5)P_3$ without the carrier caused no preferential growth cone turning, indicating that incorporation into the cytoplasmic side of the plasmalemma is necessary to induce growth cone attraction. The related phosphoinositide $PI(4,5)P_2$, when applied exogenously together with the carrier, also caused no preferential growth cone turning (Fig. 3*G*). This demonstrates that $PI(3,4,5)P_3$-induced chemoattraction is distinct rather than a general characteristic of all phosphoinositides. Application of either phosphoinositide as a gradient had no effect on the rate of axon extension (Fig. 3*H*). Thus, asymmetric $PI(3,4,5)P_3$ signaling is not only necessary for chemotactic growth cone turning induced by BDNF and netrin-1, but also sufficient by itself to elicit growth cone chemotaxis.

We next tested whether growth cone turning to the exogenous $PI(3,4,5)P_3$ gradient required Akt and PI3K activities. Application of Akti completely abolished the $PI(3,4,5)P_3$-induced attraction (Fig. 3*E–G*). Treatment with the PI3K inhibitor LY294002 attenuated the growth cone attraction induced by $PI(3,4,5)P_3$ (Fig. 3*G*), but the attenuation did not reach statistical significance (Mann–Whitney *U* test) when compared to the turning induced by either the $PI(3,4,5)P_3$ gradient or the vehicle control alone. Neither treatment affected the rate of axon extension (Fig. 3*H*). These findings indicate the critical role of downstream Akt activation during $PI(3,4,5)P_3$-induced growth cone turning.

Axon guidance *in vivo* requires asymmetric Akt activity

To further examine the role of Akt signaling in axon guidance, we used a molecular approach to dysregulate Akt function. We expressed an HA-tagged constitutively active form of Akt (CA-Akt) (Zhou et al., 2000) in the nervous system of *Xenopus* embryos by injection of mRNA (see Materials and Methods). Expression of CA-Akt caused no gross neural tube defects such as those reported after expressing a dominant-negative form of Akt (Peng et al., 2004) (data not shown). To demonstrate the effect of CA-Akt expression on spinal neuron growth cones, we used immunofluorescence to stain for pAkt and pSub (Fig. 4*A*). Quantitative measurements of both antibody staining patterns compared to a total cellular protein stain demonstrated a significant increase in phosphorylation (Fig. 4*B*). The functional growth cone turning assay revealed that expression of CA-Akt completely abolished growth cone attraction to a gradient of BDNF (Fig. 4*C,D*). Expression of CA-Akt had no effect on the rate of growth cone extension (Fig. 4*E*). Together, these results validate that expression of CA-Akt dysregulates Akt signaling in the growth cone, and support our findings with the Akt inhibitor.

To test whether dysregulated Akt signaling affects axon pathfinding *in vivo*, we assessed the guidance of commissural interneuron axons at the ventral midline during embryonic development. In this well defined model system, axons project ventrally toward the midline, guided by gradients of chemoattractant cues like netrin-1 (Fig. 5*A,B*) (Serafini et al., 1996; Kennedy et al., 2006). Commissural axons project toward the midline, which they cross at an angle slightly rostral of perpendicular. After midline crossing, they make a sharp turn rostrally and project toward targets in the brain. We expressed either the

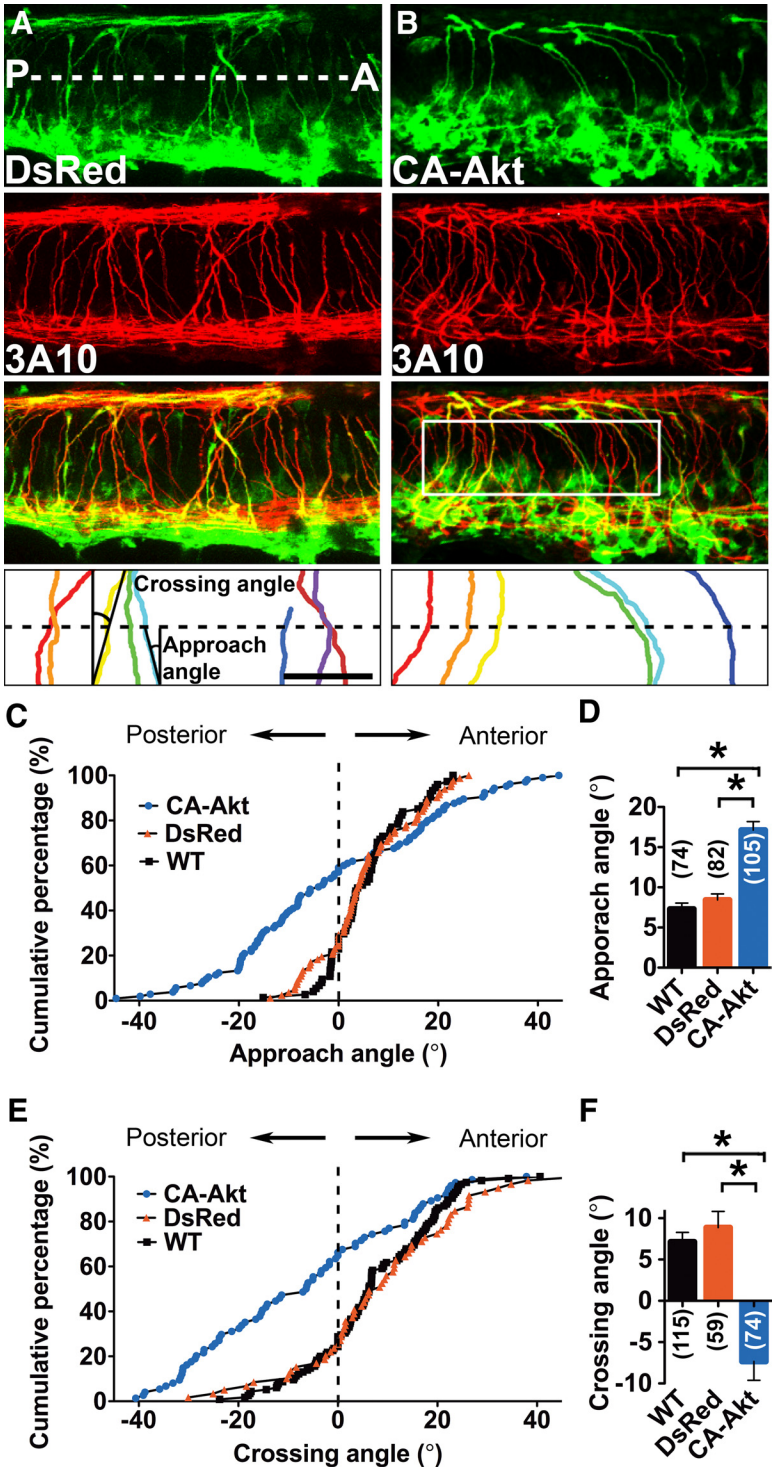

Figure 6. Dysregulated Akt signaling disrupts axon guidance *in vivo*. ***A***, Example confocal images depicting axons of commissural interneurons crossing the ventral midline of a *Xenopus* spinal cord. A control embryo was injected with DsRed mRNA at the early blastomere stage for targeted expression on one side of the nervous system and imaged at stage 27, just after labeled commissural interneuron axons have crossed the midline (green). Neural tubes were costained with antibody 3A10 to specifically label commissural interneurons (red). Dashed lines represent the ventral midline along the anterior (A) posterior (P) axis. The white box in the merged image is a 60-μm-wide example region of interest centered on the midline that was used for quantification. This is shown expanded in the bottom panel with the trajectory of double-labeled axons traced. Left and right angular arcs illustrate how the midline crossing and approach angles, respectively, of axon trajectories were measured relative to perpendicular. The origin was the center of each axon in the region of interest 30 μm proximal to the midline, and the approach and crossing endpoints were the center of each axon at the midline and 30 μm distal to the midline, respectively. Scale bars, 50 μm. ***B***, Experiments performed in the same manner as in ***A***, except that the embryo was injected with CA-Akt-HA mRNA to express constitutively active Akt, which was detected by immunostaining with an anti-HA antibody. ***C***, Cumulative frequency distribution of approach angles for each experimental condition shown in ***A*** and ***B*** compared to wild type (WT), which represents axon trajectories from the noninjected side of CA-Akt-HA-expressing embryos. ***D***, Mean approach angles (absolute values) from all experiments showing the effects of constitutively active Akt expression. ***E***, Data depicted in the same manner as in ***C***, except crossing angles were measured for each condition. ***F***, Mean crossing angles from all experiments showing the effects of constitutively active Akt expression. Data are the mean ± SEM (n = number in the parentheses). *$p < 0.05$, Mann–Whitney U test. See also Figure 5.

fluorescent protein DsRed or CA-Akt (Zhou et al., 2000) in one side of the nervous system of *Xenopus* embryos by ipsilateral injection of mRNAs (see Materials and Methods). Immunostaining with the antibody 3A10 identified commissural axons specifically (Moon and Gomez, 2005).

We first measured the approach angle of axons toward the ventral midline (0°: perpendicular to the midline; see Materials and Methods). For control axons expressing DsRed alone or noninjected wild-type axons, the mean approach angle was nearly perpendicular to the midline (8.4° ± 0.75 SEM and 7.3° ± 0.76, respectively) (Fig. 6*A*,*C*,*D*). In contrast, the mean approach angle of axons expressing CA-Akt (17.1 ± 1.1°) showed significant deviation from the control groups, with a significantly wider distribution than control axons ($p < 0.05$, F test) (Fig. 6*B–D*). The wider range of paths taken by CA-Akt-expressing axons demonstrates that these axons are less well guided to the midline. We next measured the angle of axon midline crossing in a 60 μm region centered at the midline (0°: perpendicular to the midline, anterior angles as positive, see Materials and Methods). The mean crossing angle of control DsRed and wild-type axons was anterior (8.9 ± 2.0° and 7.1 ± 1.1°, respectively) (Fig. 6*A*,*E*,*F*). In contrast, the axons expressing CA-Akt had a significantly posterior mean crossing angle (−7.3° ± 2.3), with a wider distribution of midline crossing angles compared to the controls ($p < 0.05$, F test) (Fig. 6*B*,*E*,*F*). Expression of CA-Akt also disrupted the guidance of postcrossing axons, with only 45.3% turning rostrally after midline crossing compared to 96.6% of the control DsRed-expressing axons. Thus uniform elevation of Akt activity caused significant guidance errors at the midline, supporting the notion that detection of endogenous guidance cues requires regulated Akt activation.

$PI(3,4,5)P_3$ and Akt signaling act upstream from Ca^{2+} signals

Intracellular Ca^{2+} signals mediate the effects of many chemoattractant cues, in-

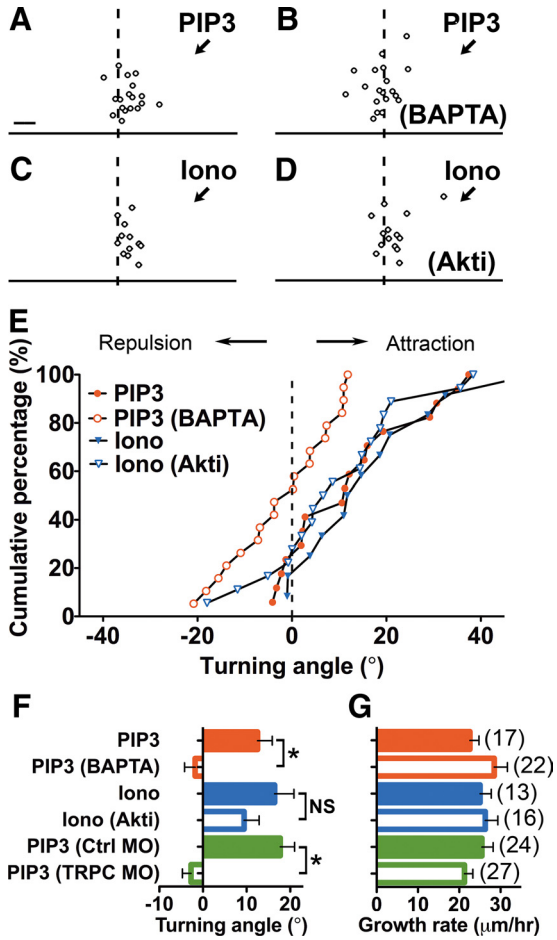

Figure 7. PI(3,4,5)P_3 signals are upstream of Ca^{2+} signals during growth cone chemoattraction. ***A–D***, Summary plots show the final position of the growth cone relative to the starting position (origin) for all experiments after 1 h treatment. The arrow marks the position of the pipette. Scale bar, 10 μm. ***A***, ***B***, Growth cones were treated with a gradient of exogenous PI(3,4,5)P_3 (PIP$_3$, 400 μM) alone (***A***) or with intracellular Ca^{2+} buffered by BAPTA-AM (1 μM) (***B***). ***C***, ***D***, Growth cones were treated with a gradient of ionomycin (Iono; 2 μM) alone (***C***), or in combination with Akti (5 μM) (***D***). ***E***, Cumulative distribution of growth cone turning angles plotted for each set of data in ***A–D***. ***F***, ***G***, Mean turning angles (***F***) and growth rates (***G***) from all experiments shown in ***A–E***, as well as data from growth cones containing a ctrl MO or TRPC MO that were treated with a PI(3,4,5)P_3 gradient. Data are the mean ± SEM (n = number in the parentheses). *$p < 0.02$; NS, not significant, Mann–Whitney U test.

cluding BDNF and netrin-1 (Hong et al., 2000; Li et al., 2005; Shim et al., 2005; Wang and Poo, 2005), and asymmetric Ca^{2+} signals in the growth cone can directly induce attractive turning (Zheng, 2000; Henley et al., 2004). However, the link between guidance receptor activation and the induction of Ca^{2+} signals during chemoattraction remains unclear. We therefore examined whether PI(3,4,5)P_3 and Akt signaling is upstream or downstream of Ca^{2+} signals. Treatment of these cultured spinal neurons with the cell permeant Ca^{2+}-buffer BAPTA-AM (1 μM) abolished the chemoattractive growth cone turning induced by a gradient of exogenous PI(3,4,5)P_3 applied in a carrier solution (Fig. 7*A*,*B*,*E*,*F*). In contrast, growth cone turning resulting from an asymmetric cytoplasmic Ca^{2+} signal, via application of a gradient of the Ca^{2+}-ionophore ionomycin in a bath solution containing defined Ca^{2+} concentration (Henley et al., 2004), persisted in the presence of Akti (Fig. 7*C–F*). Neither treatment affected the rate of axon extension (Fig. 7*G*). These findings suggest that PI(3,4,5)P_3 and Akt signaling act upstream of Ca^{2+} signals during growth cone chemotaxis.

PI(3,4,5)P_3 and Akt signaling activate growth cone TRP channels

Activation of Ca^{2+}-permeant TRP channels and the resultant Ca^{2+} influx at the growth cone of *Xenopus* spinal neurons are necessary for growth cone chemotaxis induced by netrin-1 and BDNF (Li et al., 2005; Shim et al., 2005; Wang and Poo, 2005). We therefore examined whether TRP channel activity and Ca^{2+} influx are causally linked to PI(3,4,5)P_3 signaling. We first tested whether *Xenopus* TRPC1 (xTRPC) is required for PI(3,4,5)P_3-induced chemoattraction. It has been shown previously (Wang and Poo, 2005) that injection of a specific antisense morpholino oligonucleotide in the *Xenopus* embryo (see Materials and Methods) efficiently downregulates the expression of xTRPC1 and abolishes the TRP current induced by netrin-1 in these cultured spinal neurons. We used this same antisense morpholino approach to downregulate the expression of xTRPC1 during the growth cone turning assay. Downregulating the expression of xTRPC1 by the xTRPC1 morpholino (TRPC MO) abolished growth cone attraction induced by a gradient of exogenous PI(3,4,5)P_3 plus carrier, whereas a control morpholino (Ctrl MO) had no effect (Fig. 7*F*). Neither morpholino affected the rate of axon extension (Fig. 7*G*).

To better understand the link between PI(3,4,5)P_3 and TRPC, we monitored plasmalemmal ion channel activity directly by performing whole-cell patch recordings from the growth cone (Fig. 8*A*). Perforated patch-clamp recordings of membrane potential in current-clamp mode revealed a significant depolarization induced by local application of netrin-1 from a micropipette (Fig. 8*A*,*B*), as was reported previously (Li et al., 2005; Wang and Poo, 2005). Similar local application of exogenous PI(3,4,5)P_3 in the carrier solution caused a transient membrane potential depolarization of a lower amplitude, whereas application of the carrier solution alone had no effect (Fig. 8*B*). The PI(3,4,5)P_3-induced depolarization was abolished by treatment with the TRP channel blocker SKF-96365 (25 μM) (Fig. 8*B*) (Zhu et al., 1998).

To control for potential off-target effects of SKF-96365 on other channels, we isolated TRP currents with pharmacological agents that blocked most K^+ channels, Na^+ channels, and L-, N-, P-, and T-type Ca^{2+} channels (see Materials and Methods). We then applied a voltage ramp to determine the current–voltage (I/V) relationship, and observed a small, putative TRP current in untreated growth cones (Fig. 8*C*,*D*). Local application of exogenous PI(3,4,5)P_3 in the carrier solution markedly elevated this current to a level similar to that induced by netrin-1 applied either locally by a micropipette or uniformly in the bath solution. Subsequent addition of SKF-96365 reduced the current to a level below that found before the application of PI(3,4,5)P_3. The carrier solution alone caused no change in the current compared to untreated controls (Fig. 8*D*). Local application of PI(3,4,5)P_3 in the presence of uniform bath-applied netrin-1 caused no further elevation of the putative TRP current (Fig. 8*D*), suggesting that the same channels are activated by both netrin-1 and PI(3,4,5)P_3. Using the morpholino knockdown approach (KD), we found that downregulation of xTRPC1 inhibited the putative TRP current in the growth cone induced by locally applied PI(3,4,5)P_3, whereas a control misprimed oligonucleotide (MP) had no effect on the PI(3,4,5)P_3-induced Ca^{2+} current (Fig. 8*C*,*D*). Downregulating xTRPC1 expression also attenuated the basal putative TRP currents that were detected in growth cones from the untreated and MP-treated embryos (Fig. 8*D*). These results indicate that PI(3,4,5)P_3 alone is sufficient to activate TRP channels in these spinal neurons, and thus is capable of eliciting Ca^{2+} influx that mediates chemoattractive growth cone turning.

We further examined whether the $PI(3,4,5)P_3$-induced TRP current requires PI3K and Akt activities. Treatment of the cultured spinal neurons with either LY294002 or Akti significantly attenuated the TRP current induced by a gradient of exogenous $PI(3,4,5)P_3$ applied in the carrier solution compared to the respective inhibitor alone controls (Fig. 8*C*,*D*). Treatment with Akti, SKF, or morpholino knockdown of xTRPC1 significantly attenuated the $PI(3,4,5)P_3$-induced TRP current when compared to growth cones treated with $PI(3,4,5)P_3$ alone (Fig. 8*C*,*D*). Treatment with LY294002 appeared to attenuate both the basal and $PI(3,4,5)P_3$-induced currents but was not significantly different from the respective no-inhibitor conditions (Fig. 8*D*). Altogether, these findings reveal that $PI(3,4,5)P_3$-induced activation of Akt elicits xTRPC1-dependent Ca^{2+} influx in the growth cone.

Discussion

Our findings support the following model of early signal transduction at the growth cone induced by netrin-1 and BDNF (Fig. 9): An environmental gradient of these guidance cues induces a gradient of activation of their cognate receptors at the growth cone surface membrane. Activated receptors in turn trigger the activation of PI3K (Chao, 2003; Round and Stein, 2007) and local production of $PI(3,4,5)P_3$, which accumulates asymmetrically at the plasmalemma, leading to asymmetric activation of Akt. The activated Akt in turn leads to potentiation of TRPC channels in the membrane, allowing the influx of Ca^{2+} required for triggering chemoattractive growth cone turning. Thus, asymmetric $PI(3,4,5)P_3$ signals are essential and instructive for chemotactic growth cone guidance by netrin-1 and BDNF. Furthermore, to our knowledge, this is the first demonstration that Akt signaling is critical for axon guidance. Analogous to the chemotaxis of amoeboid cells, the asymmetric membrane accumulation of $PI(3,4,5)P_3$ represents an early signal downstream of guidance receptor activation that polarizes to the leading edge during growth cone chemotaxis. Furthermore, our discovery of the $PI(3,4,5)P_3$/Akt/TRPC signaling cascade marks a novel mechanism for controlling Ca^{2+} influx. These findings on $PI(3,4,5)P_3$ and Akt signaling in the growth cone during gradient detection underscore Ramón y Cajal's vision of the growth cone as a chemotaxing amoeba and support the notion that $PI(3,4,5)P_3$

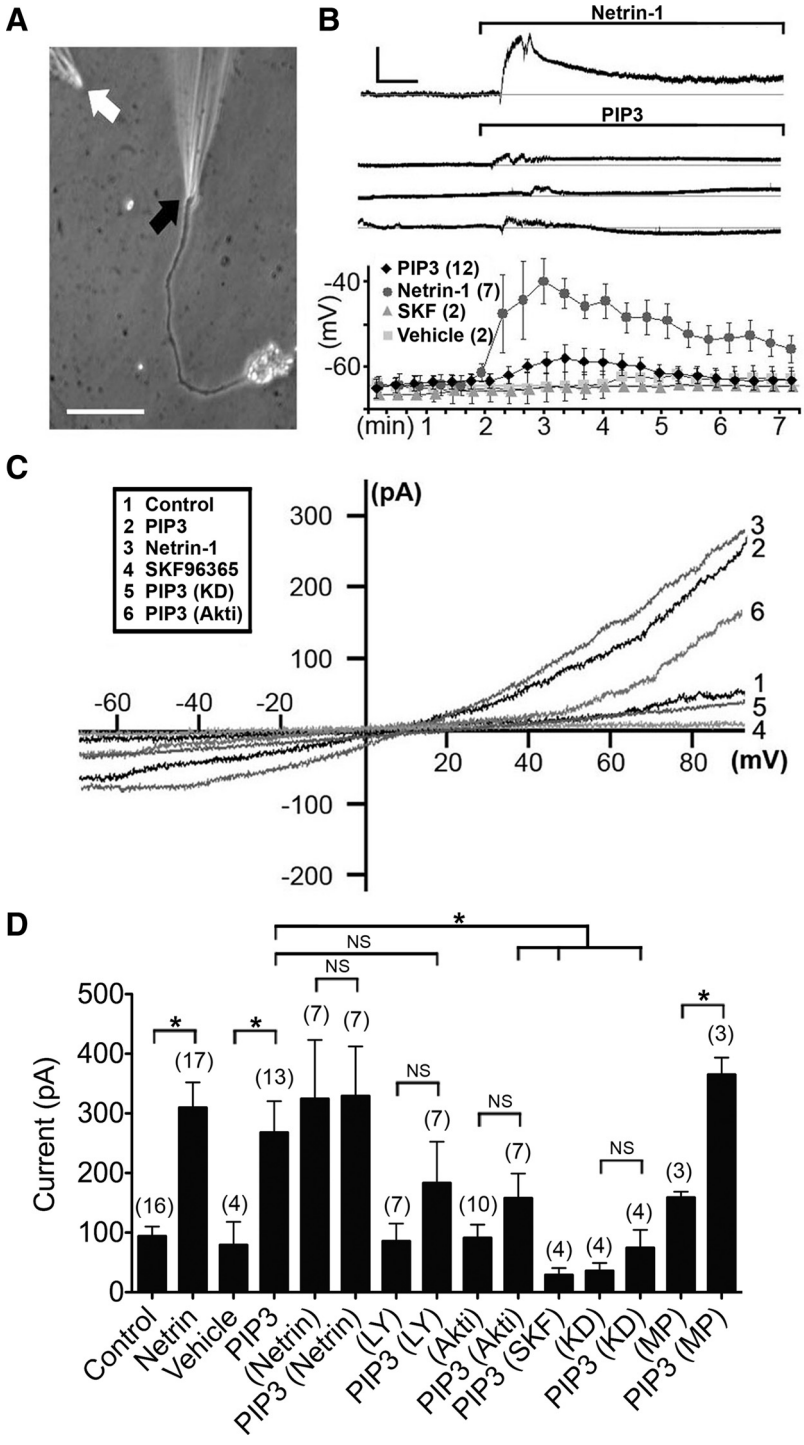

Figure 8. Activation of TRPC currents in the growth cone by a gradient of $PI(3,4,5)P_3$. ***A***, Phase-contrast image of a cultured *Xenopus* spinal neuron showing placement of a whole-cell patch recording pipette (black arrow) on the growth cone and a gradient application pipette (white arrow). Scale bar, 20 μm. ***B***, Whole-cell membrane potential recordings from individual growth cones (upper) and the means from all experiments (lower) before and after local application of netrin-1 and $PI(3,4,5)P_3$. Graph represents the mean ± SEM membrane potential as a function of time for each condition (20 s bins). Calibration: 20 mV, 40 s. ***C***, Example traces of xTRPC1 current *I/V* relationships while all major voltage-dependent channels were blocked to isolate xTRPC1 channel activity (see Materials and Methods). Traces were obtained via a 100 ms voltage ramp from −60 to 90 mV. A gradient of exogenous $PI(3,4,5)P_3$ and netrin-1 was applied via puffing pipette. Inhibitors were applied uniformly in the bath solution (see Materials and Methods). The TRP channel inhibitor SKF-96365 (25 μM) was introduced after $PI(3,4,5)P_3$ application. ***D***, Summary of all TRP current experiments. Data represent the peak current (±SEM) measured during a 100 ms step depolarization to 80 mV. Inhibitors of PI3K (LY, 30 μM) and Akti (10 μM) were added to the bath solution. Morpholino oligonucleotides to xTRPC1 (KD) and MP were injected into developing embryos at the one- to two-cell stage (see Materials and Methods). Parentheses indicate uniform application rather than as a gradient. n = number in the parentheses. *$p < 0.05$; NS, not significant (two-tailed Student's t test).

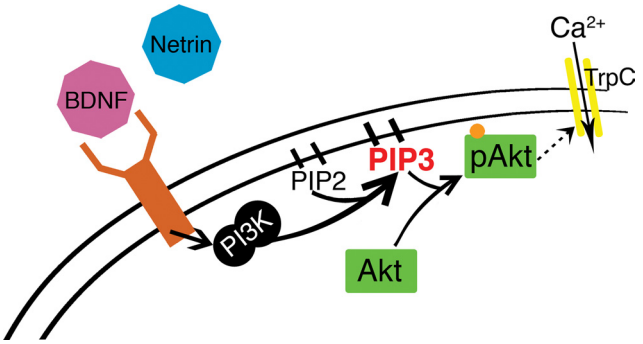

Figure 9. Model depicting the events downstream of receptor activation during growth cone chemoattraction. A gradient of chemoattractant and asymmetric receptor activation induces polarized PI(3,4,5)P_3 and Akt signals that elicit TRP channel activation and Ca^{2+} influx.

and Akt signaling is a conserved mechanism for chemotactic guidance among diverse cell types.

PI(3,4,5)P_3 regulation of TRPC

Phosphoinositides have been shown to bind and directly regulate multiple TRP channels (Kwon et al., 2007). Evidence also suggests that the BDNF receptor TrkB can gate TRP channels by a direct interaction (Bobanovic et al., 1999; Chao, 2003). Our finding that the PI(3,4,5)P_3-induced potentiation of TRPC channels in the growth cone requires Akt activity identifies a new mechanism. *Xenopus* TRPC lacks the Akt phosphorylation consensus sequence RXRXXS/T (Alessi et al., 1996), suggesting that Akt may regulate TRPC function through an intermediary. Although the molecular details remain to be defined, PI3K-dependent insertion of TRPC5 into the plasmalemma has been demonstrated in hippocampal neurons (Bezzerides et al., 2004). However, this same study showed that TRPC1, which is most similar to xTRPC by sequence homology (Bobanovic et al., 1999), is not regulated in the same manner. Whether BDNF and netrin-1 regulate xTRPC distribution at the plasmalemma awaits further investigation.

Our patch-clamp recordings demonstrated that maximal PI(3,4,5)P_3-induced activation of TRPC channels required PI3K activity, suggesting that a PI(3,4,5)P_3–PI3K positive feedback loop may regulate TRPC currents in the growth cone. We also found that inhibiting PI3K trended toward attenuating growth cone turning to a gradient of exogenous PI(3,4,5)P_3, but this did not reach statistical significance. The potential role of a feedback loop would provide a robust mechanism for breaking symmetry in the process of developing polarized growth cone responses. Indeed, cell polarization and chemotaxis in neutrophils (Weiner et al., 2002; Inoue and Meyer, 2008) requires a PI(3,4,5)P_3–PI3K positive feedback loop. However, we cannot conclusively demonstrate that such a feedback loop is required for TRPC activation and growth cone chemoattraction. It has recently been shown that photoactivated release of caged Ca^{2+} in the growth cone leads to growth cone attraction that is blocked with the PI3K inhibitor LY294002 (Akiyama and Kamiguchi, 2010). Together with our findings that PI(3,4,5)P_3 leads to Ca^{2+} influx through TRPC in the growth cone, these findings raise the possibility of a PI(3,4,5)P_3–Ca^{2+} feedback mechanism during growth cone guidance.

PI(3,4,5)P_3 as a signaling node

The early PI(3,4,5)P_3 elevation at the growth cone's leading edge is poised to function as a signaling node that coordinates the localization and activity of a diverse set of cellular machinery during growth cone chemotaxis. For example, the PI(3,4,5)P_3/Akt transduction pathway can regulate target of rapamycin (TOR)-dependent protein synthesis (Potter et al., 2002), which is required for retinal ganglion cell axon guidance (Campbell and Holt, 2001). A rapamycin-insensitive TOR complex can also affect actin dynamics in many cell types (Jacinto et al., 2004; Sarbassov et al., 2004). Therefore, whereas our findings demonstrate the Akt-dependent regulation of TRPC, Akt is likely to play additional roles in axon guidance.

It is known that PI(3,4,5)P_3 can also regulate multiple effector proteins independent of Akt. For example, PI(3,4,5)P_3 can bind and activate the detector of cytokinesis (DOCK180) family of GTP exchange factors (GEFs), which positively regulates Rac activation at the plasmalemmal leading edge in chemotaxing neutrophils (Côté et al., 2005; Nishikimi et al., 2009). Activated Rac in turn can regulate actin and membrane dynamics (Ridley, 2006), and is required for bidirectional growth cone guidance (Yuan et al., 2003). Recently, it has been demonstrated that PI(3,4,5)P_3 controls microtubule extension in the growth cone, providing yet another mechanism by which PI(3,4,5)P_3 can regulate the cytoskeleton. Thus, PI(3,4,5)P_3 can potentially function as a signaling node that directly regulates key effector proteins in addition to Akt, although the specific molecular interactions in the growth cone remain to be defined.

Removal of the 5′ phosphate from PI(3,4,5)P_3 yields another key second messenger, PI(3,4)P2. Lamellipodin binds PI(3,4)P2 and recruits Ena/VASP family members, which regulate actin dynamics (Krause et al., 2004). Null mutations of lamellipodin and Ena/VASP disrupt axon guidance in *Caenorhabditis elegans* (Chang et al., 2006). A key 5′ phosphatase that catalyzes the conversion of PI(3,4,5)P_3 to PI(3,4)P2 is the Src homology 2 domain-containing inositol-5′-phosphatase (SHIP), which is required for neutrophil chemotaxis (Nishio et al., 2007). Thus, the regulated conversion of PI(3,4,5)P_3 to PI(3,4)P2 could extend the signaling network that originates from PI(3,4,5)P_3 during growth cone chemotaxis.

Removal of the 3′ phosphate by phosphatase and tensin homolog (PTEN) converts PI(3,4,5)P_3 to PI(4,5)P_2 and suppresses PI(3,4,5)P_3/Akt signaling (Di Paolo and De Camilli, 2006). Chemotaxis in *Dictyostelium* requires PTEN, which is recruited to the plasmalemma and functions to polarize signals by excluding PI(3,4,5)P_3 from the lagging edge (Iijima and Devreotes, 2002). The role of PTEN in the spatial and temporal regulation of PI(3,4,5)P_3 signals in the growth cone remains unknown. Intriguingly, the collapsing factor semaphorin 3A induces the recruitment of PTEN to the growth cone plasmalemma (Chadborn et al., 2006), which may suppress growth-promoting PI(3,4,5)P_3 signals at the leading edge (Markus et al., 2002). Whether PTEN is recruited to the plasmalemma and facilitates polarization of PI(3,4,5)P_3 guidance signals during growth cone chemotaxis awaits further investigation.

Together, our findings have revealed that PI(3,4,5)P_3 elevation polarizes to the leading edge and may serve as an early regulator during growth cone guidance. Furthermore, we have identified PI(3,4,5)P_3 and Akt signaling as a novel link to Ca^{2+} influx in the growth cone. Potentiating Akt signaling (Namikawa et al., 2000) or downregulating PTEN expression (Park et al., 2008) can promote regenerative axon outgrowth at sites of injury. These results, together with our finding that a gradient of exogenous PI(3,4,5)P_3 can direct growth cone chemotaxis, suggest that selective manipulation of the PI(3,4,5)P_3/Akt signaling pathway may hold therapeutic promise for enhancing functional axon regeneration.

Notes

Supplemental material for this article is available at http://www.youtube.com/user/HenleyLab and consists of additional movies of the PH_{Akt}-GFP biosensor associated with the paper. These include PH_{Akt}-GFP translocation induced by insulin, BDNF, and exogenous synthetic $PI(3,4,5)P_3$. This material has not been peer reviewed.

References

Akiyama H, Kamiguchi H (2010) Phosphatidylinositol 3-kinase facilitates microtubule-dependent membrane transport for neuronal growth cone guidance. J Biol Chem 285:41740–41748.

Alessi DR, Caudwell FB, Andjelkovic M, Hemmings BA, Cohen P (1996) Molecular basis for the substrate specificity of protein kinase B; comparison with MAPKAP kinase-1 and p70 S6 kinase. FEBS Lett 399:333–338.

Bezzerides VJ, Ramsey IS, Kotecha S, Greka A, Clapham DE (2004) Rapid vesicular translocation and insertion of TRP channels. Nat Cell Biol 6:709–720.

Bobanovic LK, Laine M, Petersen CC, Bennett DL, Berridge MJ, Lipp P, Ripley SJ, Bootman MD (1999) Molecular cloning and immunolocalization of a novel vertebrate trp homologue from *Xenopus*. Biochem J 340:593–599.

Brereton HM, Harland ML, Auld AM, Barritt GJ (2000) Evidence that the TRP-1 protein is unlikely to account for store-operated Ca2+ inflow in *Xenopus laevis* oocytes. Mol Cell Biochem 214:63–74.

Campbell DS, Holt CE (2001) Chemotropic responses of retinal growth cones mediated by rapid local protein synthesis and degradation. Neuron 32:1013–1026.

Chadborn NH, Ahmed AI, Holt MR, Prinjha R, Dunn GA, Jones GE, Eickholt BJ (2006) PTEN couples Sema3A signalling to growth cone collapse. J Cell Sci 119:951–957.

Chang C, Adler CE, Krause M, Clark SG, Gertler FB, Tessier-Lavigne M, Bargmann CI (2006) MIG-10/lamellipodin and AGE-1/PI3K promote axon guidance and outgrowth in response to slit and netrin. Curr Biol 16:854–862.

Chao MV (2003) Neurotrophins and their receptors: a convergence point for many signalling pathways. Nat Rev Neurosci 4:299–309.

Côté J-F, Motoyama AB, Bush JA, Vuori K (2005) A novel and evolutionarily conserved PtdIns(3,4,5)P3-binding domain is necessary for DOCK180 signalling. Nat Cell Biol 7:797–807.

Di Paolo G, De Camilli P (2006) Phosphoinositides in cell regulation and membrane dynamics. Nature 443:651–657.

Henley J, Poo M-m (2004) Guiding neuronal growth cones using Ca2+ signals. Trends Cell Biol 14:320–330.

Henley JR, Huang K-h, Wang D, Poo M-m (2004) Calcium mediates bidirectional growth cone turning induced by myelin-associated glycoprotein. Neuron 44:909–916.

Hong K, Nishiyama M, Henley J, Tessier-Lavigne M, Poo M (2000) Calcium signalling in the guidance of nerve growth by netrin-1. Nature 403:93–98.

Iijima M, Devreotes P (2002) Tumor suppressor PTEN mediates sensing of chemoattractant gradients. Cell 109:599–610.

Inoue T, Meyer T (2008) Synthetic activation of endogenous PI3K and Rac identifies an AND-gate switch for cell polarization and migration. PLoS ONE 3:e3068.

Jacinto E, Loewith R, Schmidt A, Lin S, Rüegg MA, Hall A, Hall MN (2004) Mammalian TOR complex 2 controls the actin cytoskeleton and is rapamycin insensitive. Nat Cell Biol 6:1122–1128.

Kennedy TE, Wang H, Marshall W, Tessier-Lavigne M (2006) Axon guidance by diffusible chemoattractants: a gradient of netrin protein in the developing spinal cord. J Neurosci 26:8866–8874.

Kozikowski AP, Sun H, Brognard J, Dennis PA (2003) Novel PI analogues selectively block activation of the pro-survival serine/threonine kinase Akt. J Am Chem Soc 125:1144–1145.

Krause M, Leslie JD, Stewart M, Lafuente EM, Valderrama F, Jagannathan R, Strasser GA, Rubinson DA, Liu H, Way M, Yaffe MB, Boussiotis VA, Gertler FB (2004) Lamellipodin, an Ena/VASP ligand, is implicated in the regulation of lamellipodial dynamics. Dev Cell 7:571–583.

Kwon Y, Hofmann T, Montell C (2007) Integration of phosphoinositide- and calmodulin-mediated regulation of TRPC6. Mol Cell 25:491–503.

Li Y, Jia Y-C, Cui K, Li N, Zheng Z-Y, Wang Y-Z, Yuan X-B (2005) Essential role of TRPC channels in the guidance of nerve growth cones by brain-derived neurotrophic factor. Nature 434:894–898.

Markus A, Zhong J, Snider WD (2002) Raf and akt mediate distinct aspects of sensory axon growth. Neuron 35:65–76.

Ming G, Song H, Berninger B, Inagaki N, Tessier-Lavigne M, Poo M (1999) Phospholipase C-gamma and phosphoinositide 3-kinase mediate cytoplasmic signaling in nerve growth cone guidance. Neuron 23:139–148.

Moon M-S, Gomez TM (2005) Adjacent pioneer commissural interneuron growth cones switch from contact avoidance to axon fasciculation after midline crossing. Dev Biol 288:474–486.

Namikawa K, Honma M, Abe K, Takeda M, Mansur K, Obata T, Miwa A, Okado H, Kiyama H (2000) Akt/protein kinase B prevents injury-induced motoneuron death and accelerates axonal regeneration. J Neurosci 20:2875–2886.

Nishikimi A, Fukuhara H, Su W, Hongu T, Takasuga S, Mihara H, Cao Q, Sanematsu F, Kanai M, Hasegawa H, Tanaka Y, Shibasaki M, Kanaho Y, Sasaki T, Frohman MA, Fukui Y (2009) Sequential regulation of DOCK2 dynamics by two phospholipids during neutrophil chemotaxis. Science 324:384–387.

Nishio M, Watanabe K-i, Sasaki J, Taya C, Takasuga S, Iizuka R, Balla T, Yamazaki M, Watanabe H, Itoh R, Kuroda S, Horie Y, Förster I, Mak TW, Yonekawa H, Penninger JM, Kanaho Y, Suzuki A, Sasaki T (2007) Control of cell polarity and motility by the PtdIns(3,4,5)P3 phosphatase SHIP1. Nat Cell Biol 9:36–44.

Nishiyama M, Hoshino A, Tsai L, Henley JR, Goshima Y, Tessier-Lavigne M, Poo M-m, Hong K (2003) Cyclic AMP/GMP-dependent modulation of Ca2+ channels sets the polarity of nerve growth-cone turning. Nature 423:990–995.

Ozaki S, DeWald DB, Shope JC, Chen J, Prestwich GD (2000) Intracellular delivery of phosphoinositides and inositol phosphates using polyamine carriers. Proc Natl Acad Sci U S A 97:11286–11291.

Parent CA, Blacklock BJ, Froehlich WM, Murphy DB, Devreotes PN (1998) G protein signaling events are activated at the leading edge of chemotactic cells. Cell 95:81–91.

Park KK, Liu K, Hu Y, Smith PD, Wang C, Cai B, Xu B, Connolly L, Kramvis I, Sahin M, He Z (2008) Promoting axon regeneration in the adult CNS by modulation of the PTEN/mTOR pathway. Science 322:963–966.

Peng Y, Jiang B-H, Yang P-H, Cao Z, Shi X, Lin MCM, He M-L, Kung H-F (2004) Phosphatidylinositol 3-kinase signaling is involved in neurogenesis during *Xenopus* embryonic development. J Biol Chem 279:28509–28514.

Potter CJ, Pedraza LG, Xu T (2002) Akt regulates growth by directly phosphorylating Tsc2. Nat Cell Biol 4:658–665.

Ramón y Cajal S (1972) The structure of the retina. Springfield, IL: Thomas.

Ramsey IS, Delling M, Clapham DE (2006) An introduction to TRP channels. Annu Rev Physiol 68:619–647.

Ridley AJ (2006) Rho GTPases and actin dynamics in membrane protrusions and vesicle trafficking. Trends Cell Biol 16:522–529.

Round J, Stein E (2007) Netrin signaling leading to directed growth cone steering. Curr Opin Neurobiol 17:15–21.

Sarbassov DD, Ali SM, Kim D-H, Guertin DA, Latek RR, Erdjument-Bromage H, Tempst P, Sabatini DM (2004) Rictor, a novel binding partner of mTOR, defines a rapamycin-insensitive and raptor-independent pathway that regulates the cytoskeleton. Curr Biol 14:1296–1302.

Schweitz H, Heurteaux C, Bois P, Moinier D, Romey G, Lazdunski M (1994) Calcicludine, a venom peptide of the Kunitz-type protease inhibitor family, is a potent blocker of high-threshold Ca2+ channels with a high affinity for L-type channels in cerebellar granule neurons. Proc Natl Acad Sci U S A 91:878–882.

Serafini T, Colamarino SA, Leonardo ED, Wang H, Beddington R, Skarnes WC, Tessier-Lavigne M (1996) Netrin-1 is required for commissural axon guidance in the developing vertebrate nervous system. Cell 87:1001–1014.

Servant G, Weiner OD, Herzmark P, Balla T, Sedat JW, Bourne HR (2000) Polarization of chemoattractant receptor signaling during neutrophil chemotaxis. Science 287:1037–1040.

Shim S, Goh EL, Ge S, Sailor K, Yuan JP, Roderick HL, Bootman MD, Worley PF, Song H, Ming G-L (2005) XTRPC1-dependent chemotropic guidance of neuronal growth cones. Nat Neurosci 8:730–735.

Shim S, Yuan JP, Kim JY, Zeng W, Huang G, Milshteyn A, Kern D, Muallem S, Ming G-L, Worley PF (2009) Peptidyl-prolyl isomerase FKBP52 controls chemotropic guidance of neuronal growth cones via regulation of TRPC1 channel opening. Neuron 64:471–483.

Song HJ, Ming GL, Poo MM (1997) cAMP-induced switching in turning direction of nerve growth cones. Nature 388:275–279.

Tessier-Lavigne M, Goodman CS (1996) The molecular biology of axon guidance. Science 274:1123–1133.

Toker A, Cantley LC (1997) Signalling through the lipid products of phosphoinositide-3-OH kinase. Nature 387:673–676.

Várnai P, Balla T (1998) Visualization of phosphoinositides that bind pleckstrin homology domains: calcium- and agonist-induced dynamic changes and relationship to myo-[3H]inositol-labeled phosphoinositide pools. J Cell Biol 143:501–510.

Wang F, Herzmark P, Weiner OD, Srinivasan S, Servant G, Bourne HR (2002) Lipid products of PI(3)Ks maintain persistent cell polarity and directed motility in neutrophils. Nat Cell Biol 4:513–518.

Wang GX, Poo M-m (2005) Requirement of TRPC channels in netrin-1-induced chemotropic turning of nerve growth cones. Nature 434:898–904.

Weiner OD, Neilsen PO, Prestwich GD, Kirschner MW, Cantley LC, Bourne HR (2002) A PtdInsP(3)- and Rho GTPase-mediated positive feedback loop regulates neutrophil polarity. Nat Cell Biol 4:509–513.

Wolf AM, Lyuksyutova AI, Fenstermaker AG, Shafer B, Lo CG, Zou Y (2008) Phosphatidylinositol-3-kinase-atypical protein kinase C signaling is required for Wnt attraction and anterior–posterior axon guidance. J Neurosci 28:3456–3467.

Yuan X-b, Jin M, Xu X, Song Y-q, Wu C-p, Poo M-m, Duan S (2003) Signalling and crosstalk of Rho GTPases in mediating axon guidance. Nat Cell Biol 5:38–45.

Zheng JQ (2000) Turning of nerve growth cones induced by localized increases in intracellular calcium ions. Nature 403:89–93.

Zheng JQ, Felder M, Connor JA, Poo MM (1994) Turning of nerve growth cones induced by neurotransmitters. Nature 368:140–144.

Zhou BP, Hu MC, Miller SA, Yu Z, Xia W, Lin SY, Hung MC (2000) HER-2/neu blocks tumor necrosis factor-induced apoptosis via the Akt/NF-kappaB pathway. J Biol Chem 275:8027–8031.

Zhu X, Jiang M, Birnbaumer L (1998) Receptor-activated Ca2+ influx via human Trp3 stably expressed in human embryonic kidney (HEK)293 cells. Evidence for a non-capacitative Ca2+ entry. J Biol Chem 273:133–142.